ORIGINAL ARTICLE

Adhesion of Osteoblast-like Cells (Saos-2) on Micro-/Submicro-Patterned Apatite Scaffolds Fabricated with Apatite Cement Paste by Micro-Molding

Tsukasa AKASAKA[1], Hirofumi MIYAJI[2], Naoyuki KAGA[3], Atsuro YOKOYAMA[3], Shigeaki ABE[1], and Yasuhiro YOSHIDA[1]

[1] Department of Biomedical Materials and Engineering,
[2] Department of Periodontology and Endodontology,
[3] Department of Oral Functional Prosthodontics,
Hokkaido University Graduate School of Dental Medicine, Sapporo, Japan

Synopsis
In the present study, we developed patterned apatites with grooves, pillars, and holes by micro-molding. The effects of the patterns on adhesion of the human osteoblastic cell line Saos-2 were investigated. The patterned apatites were fabricated with apatite cement paste using the micro-molding method. The number of attached cells and ratio of cell spreading were estimated by a cell adhesion assay using Saos-2. The resulting patterns of grooves, holes, and pillars at the micro-/submicro-level were easily transferred using the corresponding mold. Saos-2 cells were well orientated on the grooves and filopodia were radially elongated on pillars. The number of attached cells on the patterned apatite was higher than that on the planar apatite. Interestingly, the tendency of increasing of ratios of spreading cells was similar to that of decreasing of water contact angle on apatite pillars. These results show that the adhesion of Saos-2 cells was affected by the type and size of the apatite patterns.

Key words: *patterned apatite, micro-molding, micro/submicro, Saos-2, cell adhesion*

Introduction

Calcium phosphate materials have been widely used in several medical scaffolds and coatings of dental implants for bone tissue repair and augmentation because of their excellent osteoconductivity and osteoinductivity. Nowadays, calcium phosphate materials have been designed in various forms including nanoparticles, nanofibers, cements, and coatings in tissue engineering [1-3].

Many micro-/nano-structures composed of calcium phosphate, such as bone and teeth in the body, play an important role in bone and teeth architecture [4, 5]. The organization of collagen and hydroxyapatite (HAp) is suggested in bone architecture, where nanohydroxyapatites are oriented to organic collagen fibers and are hierarchically organized with collagen bundles [6, 7]. Dental enamel is a highly organized array of apatite nanocrystals. It is composed of parallel

thick rods with approximate lengths of 5 μm, which are called prisms, and the rods consist of well-arranged apatite nanocrystals [8, 9]. Further, it is possible to see many other examples of micro-/nano-structures in the body.

Surface topography is an important property of biomaterial surface [10-14]. Numerous recent studies have shown that cell adhesion, spreading, and morphology were significantly affected by surface topographical patterns. To estimate the effect of topography on bone-related cells, topographic substrates at the micro- and nano-scale of various calcium phosphates have been utilized as scaffolds for cell culture [15-18].

Several types of well-defined micro-/submicro-patterned calcium phosphates have been fabricated by the following methods: biomineralization [19, 20], sputtering [21, 22], electrophoretic deposition [23], nanoparticle hybrid [24], micro-machining [25], and micro-molding [26, 27]. However, it is difficult to fabricate the patterned calcium phosphates at the nano- or submicro-level because of their hard and brittle characteristics. Alternative methods to fabricate smaller patterns with calcium phosphate will be required.

Micro-/nano-molding involving nanoimprinting [28, 29] is one of the candidates for the fabrication of scaffolds with micro-/nano-structures for cell culture. Molding methods can produce three-dimensional patterns easily via light curing, thermal pressing [30], or room temperature curing [31] and is suited for repeatedly fabrication. Although molding for patterning calcium phosphate has been developed at the micro-level, molding to pattern calcium phosphate has not been reported at the submicro- or nano-level. Therefore, the effects of patterned calcium phosphates at the submicro- or nano-level on cell behavior have not been investigated.

In the present study, we developed apatite scaffolds with micro-/submicro-scale patterns of grooves, pillars, and holes by micro-molding with apatite cement paste. The effects of the size and type of the apatite patterns on adhesion of the human osteoblastic cell line Saos-2 were investigated.

Materials and Methods

1. Preparation of the patterned apatite by micro-molding

The silicon master molds were purchased from Kyodo International Inc. (Kawasaki, Japan). The five areas of 5 × 5 mm^2 used in this study were patterned with grooves (widths of both ridges and grooves were 2 μm), holes (both pitch and diameter were 2 μm), and pillars (both pitch and diameter were 2 μm, 1 μm, or 500 nm) at a height or depth of 2 μm. Replicas of the master molds were prepared by curing of the photo-curable resin PAK-01 (Toyo Gosei Co., Ltd., Tokyo, Japan) pressed on polyethylene terephthalate films with the silicon master mold using a UV nanoimprinter (EUN-4200, Engineering System Co., Ltd.,
Nagano, Japan) at a pressure of 0.4 MPa. Next, polydimethylsiloxane (PDMS) prepolymer (KE-106 and CAT-RG, 10:1 mix; Shin-Etsu Chemical, Tokyo, Japan) [32] was cast against the above-mentioned replica mold and degassed under vacuum. The PDMS was then heat-cured at 60°C for 12 h, and then at 150°C for 30 min. Upon peeling off the cured polymer, the patterns from the replica mold were transferred to PDMS.

The preparation of patterned apatite scaffolds followed part of the method of 3D powder printing with calcium phosphate cement reported by Gbureck [33] and the method of ceramic micro-patterning reported by Holthaus [27]. One gram of α-tricalcium phosphate powder (α-TCP, approximately 5 μm in diameter; Taihei Chemical Industrial Co., Ltd., Osaka, Japan) was mixed with 0.65 mL of 0.6 M phosphoric acid solution at a 1.54 powder-to-liquid ratio (wt/wt) for 4 min. Subsequently, apatite cement paste was packed into an acryl frame of 25 × 25 × 1 mm^3 on the patterned PDMS mold and retained to cure and dry for three days at 26°C. The resulting patterned apatite was carefully peeled off from the PDMS mold. Prior to cell culture, both sides of the apatite scaffolds were sterilized under UV irradiation for 20 min.

2. Characterization of the patterned apatite surface

The chemical structure of the patterned apatite was analyzed by Fourier transform infrared (FT-IR) spectroscopy. The resulting apatite was milled with KBr powder and pressed into transparent pellets. The IR absorption spectra were obtained in the

transmission mode on a JASCO FT/IR-300E Fourier transform infrared spectrometer (JASCO Corp., Tokyo, Japan). α-TCP (described above) and commercial hydroxyapatite nanoparticles (HAp, SofSera Corp., Tokyo, Japan) were used as a control.

The surface morphology of the patterned apatite was observed under a scanning electron microscope (SEM; S-4000; Hitachi High-Tech Fielding Corp., Tokyo, Japan). Prior to imaging with SEM, the fully dried apatite was coated with Pt-Pd by a sputtering apparatus (E-1030; Hitachi High-Tech Fielding Corp., Tokyo, Japan) and immediately observed to avoid moisture absorption.

3. Wettability of the patterned apatite surface

To estimate the surface wettability [34] of the patterned apatite, 0.7-μL of ultrapure water (Kanto Chemical Co., Inc., Tokyo, Japan) were placed on the surface of the patterned apatite at 26°C and 20% humidity. Contact angles were measured at least six times on the same sample by the contact angle meter (DMs-200; Kyowa Interface Science Co., Ltd., Saitama, Japan). Images of water spreading were recorded with a CCD camera after 5 s and automated contact angles were measured using FAMAS software (Kyowa Interface Science Co., Ltd., Saitama, Japan).

4. Cell adhesion assay

To estimate cell adhesion on the patterned apatite scaffolds using osteoblast-like Saos-2 cells, we carried out a cell adhesion assay as previously reported [35]. Briefly, the patterns were immersed in PBS for 1 h and washed with PBS to remove the unreacted phosphoric acid. Then, they were pre-coated in Dulbecco's modified Eagle's medium (DMEM; Sigma-Aldrich, MO, USA) containing 10% fetal bovine serum (CELLect^{TM} GOLD; MP Biomedicals, CA, USA) and 1% penicillin-streptomycin-amphotericin B suspension (Wako Pure Chemical Industries, Ltd., Osaka, Japan) at 37°C in a humidified 5% CO_2/95% air atmosphere for 1 h. After the patterned apatite scaffolds were placed in freshly medium, Saos-2 cells were seeded at a density of 66,000 cells/cm^2 and incubated for 1 h.

To assess the cell adhesion on the patterns, the attached cells were counted from SEM images. The patterns were rinsed with PBS to remove the non-adhering cells, fixed with a solution of 2.5% glutaraldehyde, and then dehydrated following critical-point drying. The number of attached cells was counted from 15 different random fields of 396 × 315 μm^2/field of each pattern on the scaffolds from the SEM images. Results are presented as mean ± standard deviation (SD) of six experiments. To assess the spreading of the attached cells on the scaffolds, 230 to 400 attached cells on each pattern were divided into two shapes from the SEM images: (a) round, cells were spherical in appearance; (b) spread, cells extended their plasma membrane.

5. Statistical analysis

Statistical analysis was performed using GraphPad Prism version 6.05 (GraphPad software, CA, USA). All data are presented as the mean ± SD. Statistical differences were assessed by one-way ANOVA and Tukey multiple comparison post-hoc test. A value of $p < 0.05$ was considered statistically significant.

Results

1. Preparation and characterization of the patterned apatite

The patterned apatites at the micro- and submicro-level were prepared by micro-molding with apatite cement paste as illustrated in Figure 1. SEM images of the surfaces of the resulting patterns are shown in Figure 2. Patterned grooves and holes of approximately 2 μm in width and pillars of approximately 0.5 μm to 2 μm in diameter were roughly transferred from the shape in the corresponding mold. In detail, the surface of each pattern was slightly rough and not the smooth at the nano-level because it was formed by small apatite crystals. The actual diameters of feature were measured from the SEM images. The diameter of the concave grooves and holes was about 2.2 μm, indicating an enlargement of 1.1 times from the mold, which has a diameter of 2 μm. The diameter of the convex ridges and pillars was approximately 1.8 μm, indicating a shrinkage of 0.9 times from the mold, which had a diameter of 2 μm diameter. These results indicate that the volume of apatite cement paste shrunk slight while solidifying. Additionally, some defects were observed in pillars, especially in smaller apatite pillars with a diameter of 0.5 μm (Figure 2f). Defects in the underfilling apatite were also occasionally observed (Figures 5 d and 5e).

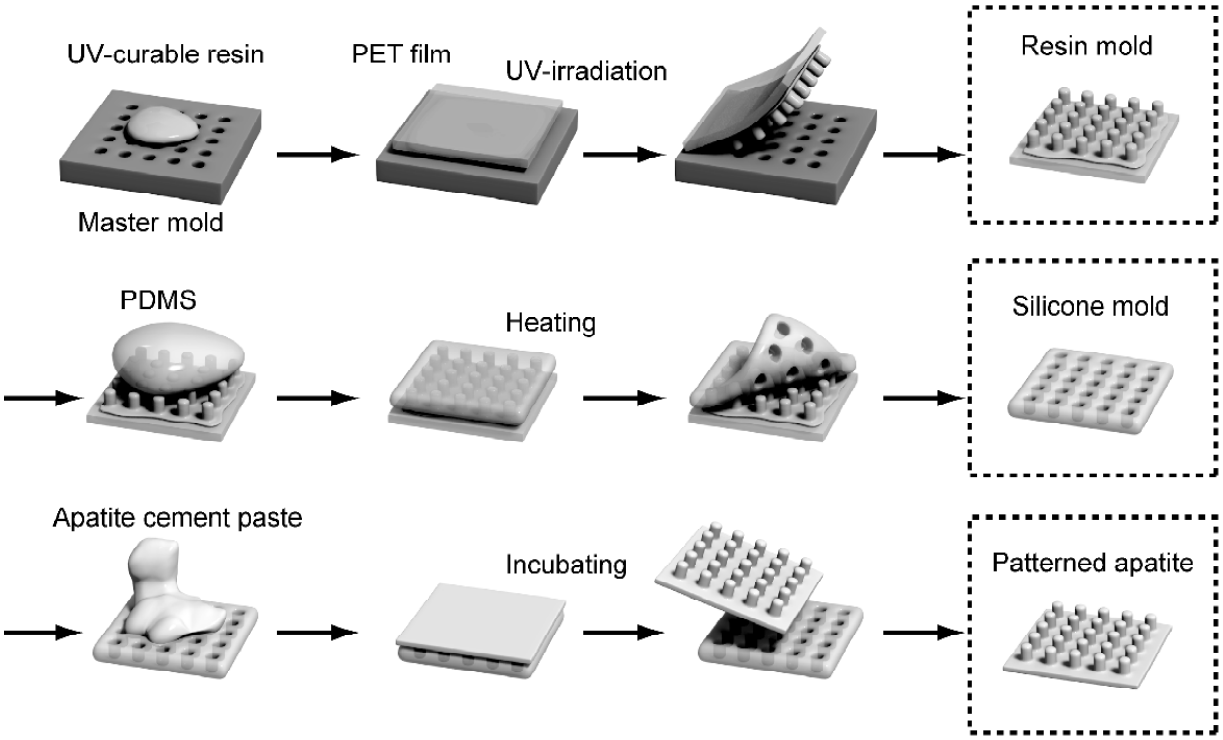

Fig. 1 An illustration of the procedure for the preparation of the micro-/submicro-patterned apatite.

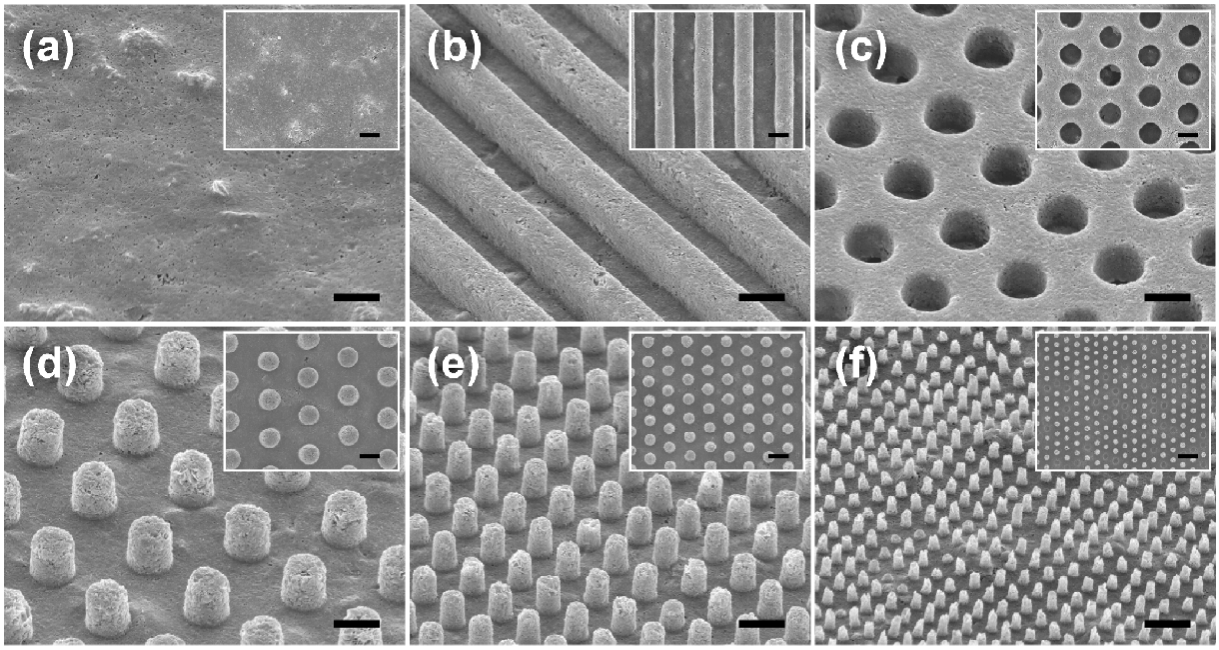

Fig. 2 SEM images of the surface of patterned apatite at an angle of 45 degrees. Insets show top-view images of the surface of the pattern. (a) Planar, (b) 2-μm grooves, (c) 2-μm holes, (d) 2-μm pillars, (e) 1-μm pillars, and (f) 0.5-μm pillars. Scale bar: 2 μm.

Figure 3 shows the FT-IR spectra of the patterned apatite. Both α-TCP and HAp were used as a controls (Figures 3b and 3c). The spectrum of the patterned apatite exhibited that OH band or associated water molecule as a weak broad peak at approximately 3400 cm^{-1}. Adsorption bands at 566 and 602 cm^{-1} and between 900 and 1100 cm^{-1} represent the PO_4^{3-} groups. The peaks of the patterned apatite (Figure 3a) were comparatively broad compared to those of highly crystalline HAp (Figure 3c). Some peaks of patterned apatite were similar to those of HAp [36] and α-TCP [37, 38], but the spectra could indicate a mixture of several calcium phosphates, including amorphous calcium phosphate [39, 40], dicalcium phosphate [33, 41, 42], and unreacted TCP. The FT-IR spectra of patterned apatite indicated that α-TCP partially reacted with phosphoric acid and formed a matrix of CaP while solidifying.

2. Contact angle on the patterned apatite surface

Figure 4 shows the water contact angles on the surface of the patterned apatite. The contact angles of the patterned apatites were in the range

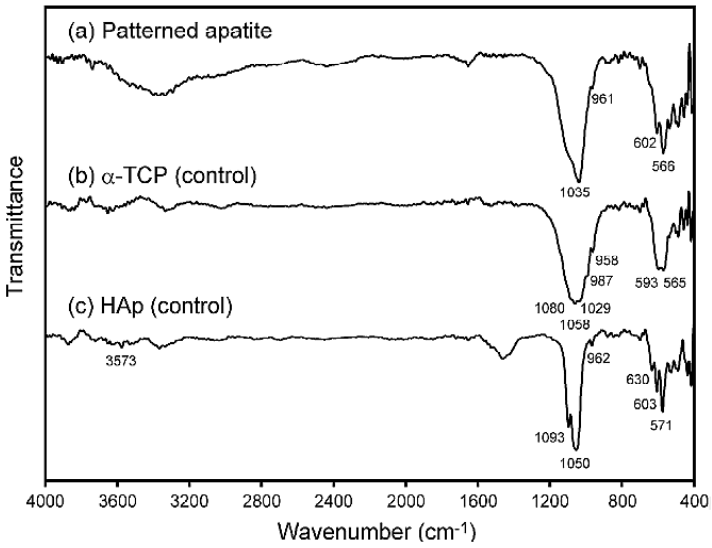

Fig. 3 FT-IR spectra of the patterned apatite. (a) Patterned apatite, (b) α-TCP (control), and (c) HAp (control).

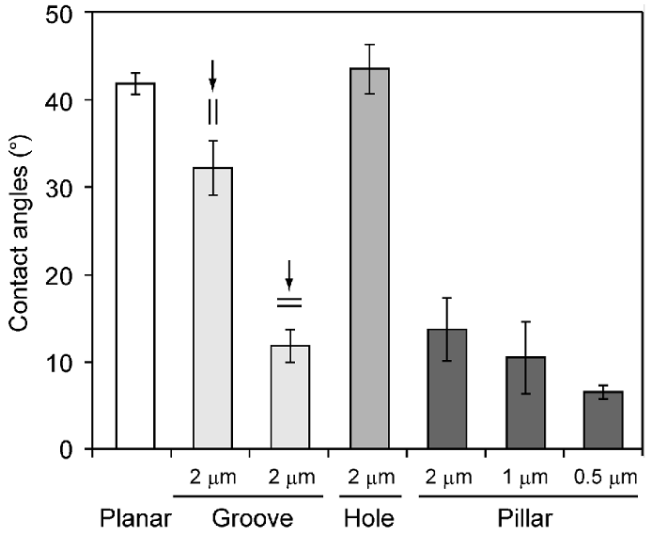

Fig. 4 Water contact angles on the patterned apatite. Arrows indicate the direction of observation relative to the direction of grooves.

of 7°–44°, while that of planar apatite was 41.8 ± 1.2°. Thus, the surface of all patterned apatites exhibited hydrophilicity. Patterning of apatite caused a decrease in the contact angle on the apatite surface. Only the contact angle of patterned holes was similar to that of planar apatite. The contact angles of grooves viewed from the horizontal and vertical direction relative to the grooves were 32.2 ± 3.1° and 12 ± 1.9°, respectively. Interestingly, smaller diameters of the patterned pillars within the range of the diameters in this study resulted in smaller contact angles.

3. Cell adhesion on the patterned apatite

The patterned apatite demonstrated better cell adhesion and spreading than did the planar apatite (Figures 5 and 6). The typical morphology of the cells attached on the patterned apatite is shown in Figure 5. The shape of the cells on the planar apatite and holes were round (Figures 5a and 5c), while the shape of the cells on the grooves was elongated along the direction of the grooves (Figure 5b). The cells on the pillars exhibited randomly elongated filopodia and lamellipodia from the spreading cells (Figures 5d–5f). The filopodia of the cells seemed to hold onto the top of the pillars. Furthermore, the cells on the smaller pillars ranging from 2 μm to 0.5 μm in diameter were better spread.

The ratio of the spread cells in the attached cells is shown in Figure 6a. The ratio of spread cells (35.8 ± 3.9%) was lower than that of round cells (64.2 ± 3.9%) on planar apatite. On the other hand, the ratio of spread cells (60.3–80.1%) was higher than that of round cells (20.0–39.9%) on the patterned apatite. The ratio of spreading cells on the patterned apatite was significantly higher than that on the planar surfaces ($p < 0.05$). However, there are no significantly differences ($p > 0.05$) among the patterns. Interestingly, among the pillars, the cells on the pillars with smaller diameters showed higher ratios of spreading cells, but the difference was

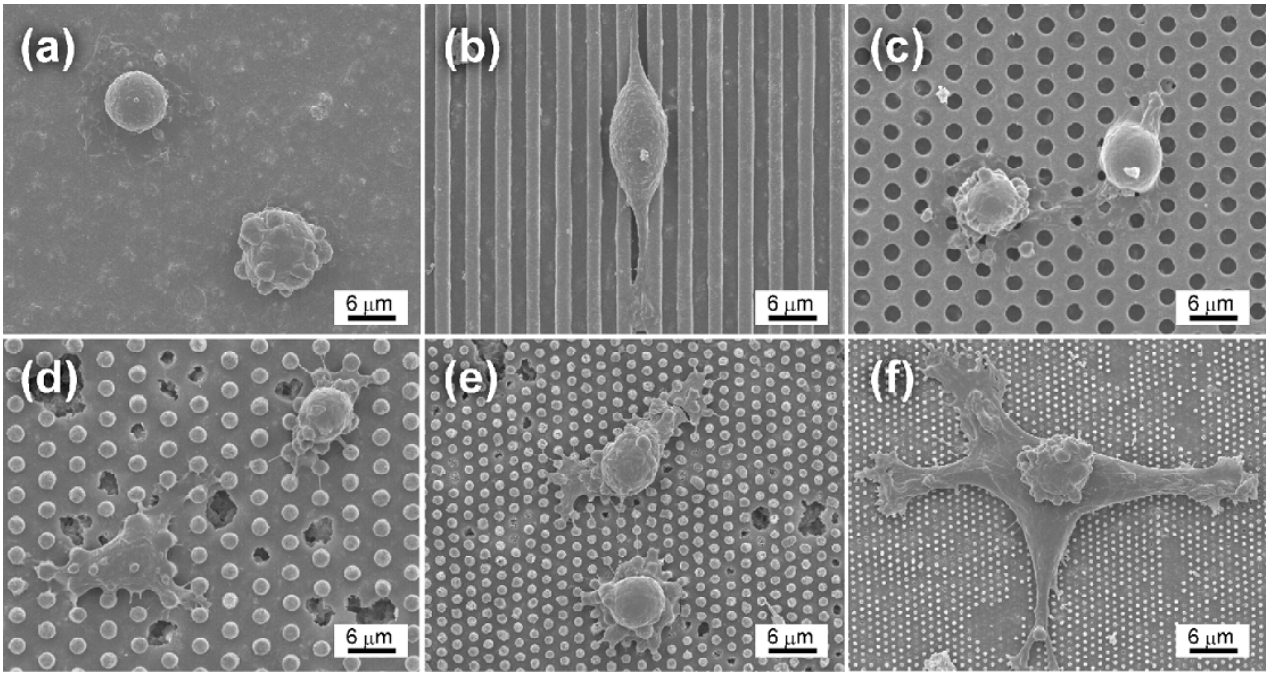

Fig. 5 SEM images of attached Saos-2 cells on the micro-/submicro-patterned apatite after 1 h of incubation. (a) Planar, (b) 2-μm grooves, (c) 2-μm holes, (d) 2-μm pillars, (e) 1-μm pillars, and (f) 0.5-μm pillars.

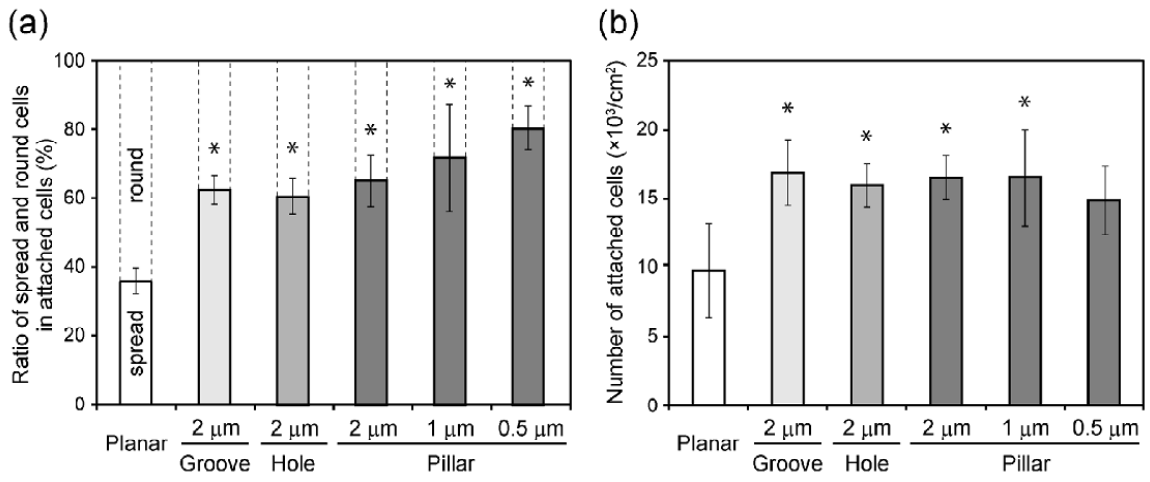

Fig. 6 Cell adhesion assay of Saos-2 cells on the patterned apatite. (a) Ratio of the spread and round cells in the attached cells. (b) Number of attached cells. Statistical difference in comparison with the planar group as a control was analyzed by one-way ANOVA followed by Tukey multi-comparison test (* indicates $p < 0.05$).

not significant ($p > 0.05$).

Figure 6b shows the numbers of attached cells on the patterns. The number of attached cells on the patterns, aside from pillars with a diameter of 0.5 μm, was approximately 1.5–1.7 times higher ($p < 0.05$) than that on planar apatite. There were no significantly differences ($p > 0.05$) among the patterns.

Discussion

1. Preparation of patterned apatites by micro-molding

The patterned apatites were fabricated by micro-molding with apatite cement paste to improve CaP patterning and estimate cell adhesion ability. Patterns of grooves, holes, and pillars were formed according to the corresponding mold of each size and shape (Figure 2). After a portion of α-TCP powder was dissolved in H_3PO_4 solution, patterned apatite was formed by crystallization or solidification of apatite cement paste inside the patterned space of the PDMS mold. It is easy for apatite cement paste to enter in the patterned space of the PDMS mold, but the patterned apatite shrunk while solidifying. The resulting patterned apatite could be composed of a mixture of some calcium phosphate compounds (Figure 3). The patterned apatite had a rough surface that consisted of apatite crystals at the nano-level (Figure 2).

The patterns that were 2 μm in diameter were more easily fabricated than those that were 1 μm or 0.5 μm in diameter. Moreover, it was difficult to fabricate patterns with smaller diameters with no defects in the entire patterned area. In particular, the defects were partially observed in pillars with smaller diameter pillars (Figure 2f). Apatite pillars could be broken because of their hardness and brittleness when peeling the patterned apatite from the silicone mold. Additionally, defects seemed to form more easily apatite pillars than in grooves and holes. In the future, we will attempt to develop stronger patterned apatite.

Many researchers have reported methods of fabricating patterned apatites of various sizes. Holthaus et al. reported fine micro-patterns ranging from 5 μm to 140 μm made by micro-molding with hydroxyapatite powder and/or binder [25-27]. Their method can be used to fabricate crack-free patterned apatite body and is applicable for large-area micro-printing. Yang et al. reported that calcium phosphate micro-patterns were fabricated by coating a silicon wafer mold with calcium phosphate via a spattering system [21]. Tan et al. [19] and Klymov et al. [20] reported that hierarchically micro- and nano-structures of apatite coating were fabricated by mineralization from calcium phosphate solution. The resulting surfaces of the silicon or

polystyrene substrates were patterned with apatite at the micro- and submicro-level. These spattering and coating methods make it possibility to fabricate apatite patterns at the submicro- and nano-scale. Hereafter, methods to fabricate smaller apatite patterns will be required.

In this study, we tried to fabricate patterned substrates composed of apatite only from apatite cement paste by room-temperature micro-molding. Our method could has advantages in the fabrication of apatite body with micro- and submicro-sized patterns. Furthermore, it is applicable in the fabrication of patterned dental materials via solidification from temporary paste with conventional dental materials such as apatite cement and glass ionomer cements (data not shown). In the future, patterned dental materials may be directly fabricated on the surface of teeth for one of dental treatments, by using our method.

2. Cell adhesion of Saos-2 on the patterned apatite

The adhesion and morphology of Saos-2 cells were affected by the type and size of the patterns on the surface of the apatite scaffolds. Our results of Saos-2 orientation in the direction of apatite grooves are in agreement with the results for osteogenic cells such as human osteoblasts (HOB) [26], human fetal osteoblasts (hFOB) [21], Saos-2 and MG63 [22, 19], and MC3T3-E1 [20]. In the studies above, well-aligned cells were reported on grooves with widths between 300 nm to 60 μm on various CaP substrates. In particular, our results on the apatite grooves with a width of 2 μm are very similar to the results of hFOB on similar grooves with a width of 3 μm on CaP micro-patterns [21]. The cell area and elongation on grooves was higher than those on planar apatite, and the spherical morphology of cells on planar apatite was also similar. Several researchers reported that the grooves with narrow widths, from the submicro-level to several tens of micron, are effective in controlling the orientation and elongation of cells compared to grooves with wider widths, from tens to hundreds of microns [22, 26]. These reports supported that the narrow size of our grooves are suitable for cell orientation on apatite scaffolds. Additionally, it is known that other factors including hydrophilicity [43] and serum adsorption [44] have an influence on cell orientation. These factors also contribute to the alignment of cells on our apatite grooves. Therefore, the adequate shape and size of patterns would be one of the important factors in controlling the morphology or orientation of the cells on the apatite patterns.

Saos-2 cells on pillar patterns exhibited radially elongated filopodia. Cells on pillars with smaller diameters in the range of 0.5 μm to 2 μm seemed to exhibit larger cell areas (Figures. 5d–5f). The tips of the filopodia were holding onto the top of the pillars, an observation similar to that reported previously [43, 45]. Saos-2 cells held onto the top of carbon nitride coating pillars and spread to neighboring pillars [43]. Furthermore, numerous filopodia of Saos-2 cells extended radially and held onto the top of smaller PLLA pillars with a diameter of 200 nm and a pitch of 1 μm [45]. Interestingly, the tendency of increasing ratio of spreading cells (Figure 6a) was similar to the tendency of decreasing water contact angle on apatite pillars (Figure 4). On the other hand, it was reported that Saos-2 cells or HeLa cells on hydrophobic pillar patterns were not well spread [43, 46]. Therefore, surface hydrophilicity, especially enhanced hydrophilicity, of the patterned apatite could be preferable for large cell spreading.

The number of attached Saos-2 cells on the patterned apatite was about 1.7–2.2 times higher than that on the planar apatite at the early stage (Figure 6b). However, there were no significantly differences among the patterned apatites. Interestingly, there is no correlation between the contact angle (Figure 4) and the number of attached cells; however, correlation was seen between the contact angle and the ratio of spread cells on the patterns, especially on pillars (Figure 6a). The increased number of attached Saos-2 cells on our apatite patterns compared to that on planar apatite is similar to the increased number of cells on carbon nitride-coating pillars with a diameter of 20 μm [43] and on the polylactic acid pillars with a diameter of 200 nm [45] compared to corresponding planar surfaces. In addition, Saos-2 cells showed the same tendency of increased attachment on the patterns, but bone marrow stem cells showed the opposite tendency

of decreased attachment on the patterns [45]. The different behavior of cells on patterns indicates that cell type is an important factor in determining cell attachment. Further, Myllymaa et al. suggested that surface topography and surface free energy are two important factors that regulate cell response to biomaterials, and increased wettability has been shown to enhance cell attachment [43]. In our case, Saos-2 cells preferred the patterned apatites with widths or diameters in the range of 0.5–2 μm rather than planar apatite because of adequate hydrophilicity and roughness.

On the other hand, our results disagree with those in a previous report that indicated no significant difference in Saos-2 cell adhesion on hierarchically micro/nano apatite patterns and planar surfaces after a 4-hour incubation [19]. We speculate that the difference in adhesion could be caused by different micro-/nano-structures or differences in wettability. In the future, it is necessary to search for factors responsible for the correlation between cell adhesion and patterns in detail.

Conclusion

We prepared patterned apatites without a binder from apatite cement paste by micro-molding at room temperature. The resulting patterns of grooves, holes, and pillars at the micro/submicro-level were easily transferred, according to the corresponding mold of each size and shape with slight shrinkage while solidifying. However, defects were partially observed in a portion of the smaller pattern area, especially within smaller pillars. The results show that this method is sufficient for the preparation of apatite grooves, holes, and pillars with widths or diameters of 2 μm. Further improvement is necessary for smaller pillars with diameters below 1 μm, because of their brittle nature.

To estimate cell adhesion on the patterned apatite scaffolds, we carried out cell adhesion assays using osteoblast-like Saos-2 cells. Saos-2 cells were well orientated on the grooves, and filopodia were elongated radially on the pillars. The number of attached cells on the patterned apatite was higher than that on the planar apatite. Interestingly, the tendency of increasing ratio of spread cells was similar to that decreasing water contact angle on apatite pillars. These results show that adhesion and morphology of Saos-2 cells were affected by the type and size of the patterns on the surface of apatite scaffolds.

Acknowledgments

This work was partly funded by “Adaptable and Seamless Technology Transfer Program through Target-driven R&D” Grant Number (No. AS251Z00599P) from the Japan Science and Technology (JST), by Suharakinenzaidan Co., Ltd., and by JSPS KAKENHI Grant Number (No. 25463047).

References

1) LeGeros RZ. Calcium phosphate-based osteoinductive materials. Chem Rev 2008; 108: 4742-4753.
2) Bose S, Tarafder S. Calcium phosphate ceramic systems in growth factor and drug delivery for bone tissue engineering: A review. Acta Biomater 2012; 8: 1401-1421.
3) Zakaria SM, Zein SHS, Othman MR, Yang F, Jansen JA. Nanophase hydroxyapatite as a biomaterial in advanced hard tissue engineering: a review. Tissue Eng Part B Rev 2013; 19: 431-441.
4) Chen PY, McKittrick J, Meyers MA. Biological materials: Functional adaptations and bioinspired designs. Prog Mater Sci 2012; 57: 1492-1704.
5) Palmer LC, Newcomb CJ, Kaltz SR, Spoerke ED, Stupp SI. Biomimetic Systems for Hydroxyapatite Mineralization Inspired By Bone and Enamel. Chem Rev 2008; 108: 4754-4783.
6) Lakes R. Materials with structural hierarchy. Nature 1993; 361: 511-515.
7) Luz GM, Mano JF. Mineralized structures in nature: Examples and inspirations for the design of new composite materials and biomaterials. Composites Sci Technol 2010; 70: 1777-1788.
8) Cui FZ, Ge J. New observations of the hierarchical structure of human enamel, from nanoscale to microscale. J Tissue Eng Regen Med 2007; 1: 185-191.
9) Eimar H, Ghadimi E, Marelli B, Vali H, Nazhat SN, Amin WM, Torres J, Ciobanu O, Albuquerque Junior RF, Tamimi F. Regulation of enamel hardness by its crystallographic dimensions. Acta Biomater 2012; 8: 3400-3410.
10) Nikkhah M, Edalat F, Manoucheri S, Khademhosseini A. Engineering microscale topographies to control the cell-substrate interface. Biomaterials 2012; 33: 5230-5246.
11) Biggs MJP, Richards RG, Dalby MJ. Nanotopographical modification: a regulator

of cellular function through focal adhesions. Nanomedicine 2010; 6: 619-633.
12) Martínez E, Engel E, Planell JA, Samitier J. Effects of artificial micro- and nano-structured surfaces on cell behaviour. Ann Anat 2009; 191: 126-135.
13) Anselme K, Davidson P, Popa AM, Giazzon M, Liley M, Ploux L. The interaction of cells and bacteria with surfaces structured at the nanometre scale. Acta Biomater 2010; 6: 3824-3846.
14) Jeon HJ, Simon CG, Kim GH. A mini-review: Cell response to microscale, nanoscale, and hierarchical patterning of surface structure. J Biomed Mater Res Part B, Appl Biomater B 2014; 102: 1580-1594.
15) Ivanovski S, Vaquette C, Gronthos S, Hutmacher DW, Bartold PM. Multiphasic Scaffolds for Periodontal Tissue Engineering. J Dent Res 2014; 93: 1212-1221.
16) Bruinink A, Bitar M, Pleskova M, Wick P, Krug HF, Maniura-Weber K. Addition of nanoscaled bioinspired surface features: A revolution for bone-related implants and scaffolds? J Biomed Mater Res Part A 2014; 102: 275-294.
17) Zan X, Sitasuwan P, Feng S, Wang Q. Effect of Roughness on in Situ Biomineralized CaP-Collagen Coating on the Osteogenesis of Mesenchymal Stem Cells. Langmuir 2016; 32: 1808-1817.
18) Lee SY, Yun HM, Perez RA, Gallinetti S, Ginebra MP, Choi SJ, Kim EC, Kim HW. Nanotopological-tailored calcium phosphate cements for the odontogenic stimulation of human dental pulp stem cells through integrin signaling. RSC Adv 2015; 5: 63363-63371.
19) Tan J, Saltzman WM. Biomaterials with hierarchically defined micro- and nanoscale structure. Biomaterials 2004; 25: 3593-3601.
20) Klymov A, Song J, Cai X, te Riet J, Leeuwenburgh S, Jansen JA, Walboomers XF. Increased acellular and cellular surface mineralization induced by nanogrooves in combination with a calcium-phosphate coating. Acta Biomater 2016; 31: 368-377.
21) Yang SP, Yang CY, Lee TM, Lui TS. Effects of calcium-phosphate topography on osteoblast mechanobiology determined using a cytodetacher. Mater Sci Eng C 2012; 32: 254-262.
22) Lu X, Leng Y. Quantitative analysis of osteoblast behavior on microgrooved hydroxyapatite and titanium substrata. J Biomed Mater Res A 2003; 66: 677-687.
23) Wang R, Hu YX. Patterning hydroxyapatite biocoating by electrophoretic deposition. J Biomed Mater Res A 2003; 67: 270-275.
24) Carvalho A, Pelaez-Vargas A, Gallego-Perez D, Grenho L, Fernandes MH, De Aza AH, Ferraz MP, Hansford DJ, Monteiro FJ. Micropatterned silica thin films with nanohydroxyapatite micro-aggregates for guided tissue regeneration. Dent Mater 2012; 28: 1250-1260.
25) Holthaus MG, Twardy S, Stolle J, Riemer O, Treccani L, Brinksmeier E, Rezwan K. Micromachining of ceramic surfaces: Hydroxyapatite and zirconia. J Mater Process Technol 2012; 212: 614-624.
26) Holthaus MG, Stolle J, Treccani L, Rezwan K. Orientation of human osteoblasts on hydroxyapatite-based microchannels. Acta Biomater 2012; 8: 394-403.
27) Holthaus MG, Kropp M, Treccani L, Lang W, Rezwan K. Versatile crack-free ceramic micropatterns made by a modified molding technique. J Am Ceram Soc 2010; 93: 2574-2578.
28) Chou SY, Krauss PR, Renstrom PJ. Imprint lithography with 25-nanometer resolution. Science 1996; 272: 85-87.
29) Lima MJ, Correlo VM, Reis RL. Micro/nano replication and 3D assembling techniques for scaffold fabrication. Mater Sci Eng C 2014; 42: 615-621.
30) Kooy N, Mohamed K, Pin LT, Guan OS. A review of roll-to-roll nanoimprint lithography. Nanoscale Res Lett 2014; 9: 320.
31) Igaku Y, Matsui S, Ishigaki H, Fujita J, Ishida M, Ochiai Y, Namatsu H, Hiroshima H. Room temperature nanoimprint technology using hydrogen silsequioxane (HSQ). Jpn J Appl Phys 2002; 41: 4198-4202.
32) Torisawa Y, Takagi A, Nashimoto Y, Yasukawa T, Shiku H, Matsue T. A multicellular spheroid array to realize spheroid formation, culture, and viability assay on a chip. Biomaterials 2007; 28: 559-566.
33) Gbureck U, Hölzel T, Klammert U, Würzler K, Müller FA, Barralet JE. Resorbable dicalcium phosphate bone substitutes prepared by 3D powder printing. Adv Funct Mater 2007; 17: 3940-3945.
34) Akasaka T, Yokoyama A, Matsuoka M, Hashimoto T, Fumio F. Thin films of single-walled carbon nanotubes promote human osteoblastic cells (Saos-2) proliferation in low serum concentrations. Mater Sci Eng C 2010; 30: 391-399.
35) Akasaka T, Yokoyama A, Matsuoka M, Hashimoto T, Abe S, Uo M, Watari F. Adhesion of human osteoblast-like cells (Saos-2) to carbon nanotube sheets. Biomed Mater Eng 2009; 19: 147-153.
36) Rehman I, Bonfield W. Characterization of hydroxyapatite and carbonated apatite by photo acoustic FTIR spectroscopy. J Mater Sci: Mater Med 1997; 8: 1-4.
37) Carrodeguas RG, De Aza S. α-Tricalcium phosphate: Synthesis, properties and biomedical applications. Acta Biomater 2011; 7: 3536-3546.
38) Mestres G, Le Van C, Ginebra MP. Silicon-stabilized α-tricalcium phosphate and its

use in a calcium phosphate cement: Characterization and cell response. Acta Biomater 2012; 8: 1169-1179.
39) Combes C, Rey C. Amorphous calcium phosphates: Synthesis, properties and uses in biomaterials. Acta Biomater 2010; 6: 3362-3378.
40) Somrani S, Rey C, Jemal M. Thermal evolution of amorphous tricalcium phosphate. J Mater Chem 2003; 13: 888-892.
41) Han JK, Song HY, Saito F, Lee BT. Synthesis of high purity nano-sized hydroxyapatite powder by microwave-hydrothermal method. Mater Chem Phys 2006; 99: 235-239.
42) Destainville A, Champion E, Bernache-Assollant D, Laborde E. Synthesis, characterization and thermal behavior of apatitic tricalcium phosphate. Mater Chem Phys 2003; 80: 269-277.
43) Myllymaa K, Myllymaa S, Korhonen H, Lammi MJ, Saarenpää H, Suvanto M, Pakkanen TA, Tiitu V, Lappalainen R. Improved adherence and spreading of Saos-2 cells on polypropylene surfaces achieved by surface texturing and carbon nitride coating. J Mater Sci: Mater Med 2009; 20: 2337-2347.
44) Rezek B, Michalíková L, Ukraintsev E, Kromka A, Kalbacova M. Micro-pattern guided adhesion of osteoblasts on diamond surfaces. Sensors 2009; 9: 3549-3562.
45) Özçelik H, Padeste C, Hasirci V. Systematically organized nanopillar arrays reveal differences in adhesion and alignment properties of BMSC and Saos-2 cells. Colloids Surf B Biointerfaces 2014; 119: 71-81.
46) Nomura S, Kojima H, Ohyabu Y, Kuwabara K, Miyauchi A, Uemura T. Nanopillar sheets as a new type of cell culture dish: detailed study of HeLa cells cultured on nanopillar sheets. J Artif Organs 2006; 9: 90-96.

(Received: September 29, 2016/
Accepted: December 8, 2016)

Corresponding author*:*
Tsukasa AKASAKA, Ph.,D.
Department of Biomedical Materials
and Engineering, Hokkaido University
Graduate School of Dental Medicine,
Sapporo 060-8586, Japan
E-mail: akasaka@den.hokudai.ac.jp
Tel.: +81 706 4250
Fax: +81 706 4251